

**Designed metamagnetism in  $\text{CoMnGe}_{1-x}\text{P}_x$** Z. Gercsi,<sup>1</sup> K. Hono,<sup>2</sup> and K. G. Sandeman<sup>1</sup><sup>1</sup>*Department of Physics, Blackett Laboratory, Imperial College London, London SW7 2AZ, United Kingdom*<sup>2</sup>*Magnetic Materials Center, National Institute for Materials Science (NIMS), 1-2-1 Sengen, Tsukuba 305-0047, Japan*

(Received 12 January 2011; published 2 May 2011)

We extend our previous theoretical study of Mn-based orthorhombic metamagnets to those that possess large nearest neighbor Mn-Mn separations ( $d_1 \gtrsim 3.22 \text{ \AA}$ ). Based on our calculations, we design and synthesize a series of alloys,  $\text{CoMnGe}_{1-x}\text{P}_x$ , to experimentally demonstrate the validity of the model. Unusually, we predict and prepare several metamagnets from two ferromagnetic end-members, thus demonstrating a new example of how to vary crystal structure, within the  $Pnma$  symmetry group, to provide highly tunable metamagnetism.

DOI: [10.1103/PhysRevB.83.174403](https://doi.org/10.1103/PhysRevB.83.174403)

PACS number(s): 75.30.Sg, 75.30.Kz, 75.80.+q, 75.30.Et

**I. INTRODUCTION**

Manganese-based orthorhombic ( $Pnma$ ) binary and ternary alloys are of fundamental research interest as they often exhibit complex, noncollinear magnetic structures that can be tuned by temperature, pressure, and applied magnetic field. Some well-known examples are the set of fan, helical, and cycloidal spin structures found in the ( $H, T$ ) phase diagram of MnP,<sup>1-3</sup> the cycloidal antiferromagnetism (AFM) of  $\text{IrMnSi}$ <sup>4</sup> and helical metamagnetism of  $\text{CoMnSi}$ .<sup>3,5</sup> Various theoretical explanations have previously been suggested to describe the mechanisms responsible for the noncollinear magnetism of such materials. Some refer to competing symmetric and asymmetric exchange interactions;<sup>2,6</sup> others to conduction-mediated indirect (RKKY) exchange.<sup>7</sup> Another potential cause put forward is band crossing and appropriate Fermi surface topology (nesting).<sup>4,8</sup>

One of the most feature-rich materials of this kind is  $\text{CoMnSi}$  on account of its pronounced magnetic field-induced tricritical metamagnetism and associated negative magnetocaloric effect (MCE).<sup>9</sup> Our recent high-resolution neutron diffraction (HRPD) study<sup>10</sup> uncovered a giant magnetoelastic coupling within the antiferromagnetic ground state of this system. It occurs as a change of up to 2% in nearest-neighbor Mn-Mn separations  $d_1, d_2$  on heating. The field-induced tricriticality of this system can thus be understood as the result of tuning the metamagnetic critical temperature with an applied magnetic field to the point at which it coincides with this native giant magnetoelasticity.

Using density functional theory (DFT) we recently examined the importance of the same Mn-Mn separations in determining the occurrence of different magnetic ground states across several Mn-based orthorhombic ( $Pnma$ ) systems.<sup>11</sup> By applying hydrostatic expansion and compression to a prototype model MnP alloy, we found a stability criterion for the appearance of an AFM ground state, rather than the usual FM state seen in MnP. This direct relation between Mn-Mn separation and magnetic ground state can explain the energetic proximity of FM and AFM states in materials such as  $\text{CoMnSi}$ ,<sup>3,5</sup>  $\text{MnAs}_{1-x}\text{P}_x$ ,<sup>12</sup>  $(\text{Fe}_{1-x}\text{Co}_x)\text{MnP}$ ,<sup>13</sup> and  $\text{NiMnGe}_{1-x}\text{Si}_x$ <sup>14</sup> where the nearest-neighbor Mn-Mn distances are close to a critical separation of  $2.95 \text{ \AA} \lesssim d_1 \lesssim 3.05 \text{ \AA}$ .

Although the latter model was computed in a large interval of  $2.5 \text{ \AA} \lesssim d_1 \lesssim 3.22 \text{ \AA}$  to cover many of the relevant

compositions in the literature, it may lead to a misinterpretation of a technologically relevant alloy with a larger  $d_1 = 3.4 \text{ \AA}$  spacing:  $\text{CoMnGe}$ .  $\text{CoMnGe}$  is a collinear ferromagnet with a tendency to form a metastable hexagonal structure upon rapid cooling.<sup>15</sup> In this article, we extend our previous theoretical analysis<sup>11</sup> toward larger Mn-Mn separations to explain the reappearance of ferromagnetism in alloys with  $d_1 \gtrsim 3.37 \text{ \AA}$ . The importance of the correct theoretical description of latter composition is due its large magnetocaloric effect around room temperature.<sup>16-18</sup>

In this article we first show the striking reappearance of a FM ground state at large interatomic Mn separations in Mn-based  $Pnma$  alloys where  $d_1 \gtrsim 3.37 \text{ \AA}$ , thereby accounting for the magnetic properties of  $\text{CoMnGe}$ . Secondly, and significantly, we have designed a new alloy series,  $\text{CoMn(P,Ge)}$  based on our extended model in order to test and demonstrate its validity and in particular the dominance of the ( $d_1$ ) Mn-Mn separation in determining the magnetic ground state of the series of Mn-containing  $Pnma$  alloys. We show that metamagnetism can be derived, unusually, by interdoping two ferromagnetic end-compositions in order to bring  $d_1$  to the critical regime where antiferromagnetism and ferromagnetism are similar in energy.

The remainder of the article is organised as follows. First in Sec. II, the theoretical results calculated by applying DFT to the prototype MnP alloy are given. Based on this model, we present the structural and metamagnetic properties of purposefully designed  $\text{CoMnGe}_{1-x}\text{P}_x$  alloys in Sec. III. Finally, a summary is made and conclusions are drawn in Sec. IV.

**II. THEORETICAL**

In our previous work we considered what we term the “prototype” binary MnP ( $Pnma$ ) alloy and calculated the effect of isotropic lattice expansion and compression on hypothetical nonmagnetic (NM), ferromagnetic (FM), and antiferromagnetic (AFM) states by using the general gradient approximation method (GGA-DFT) implemented in VASP Kresse and Furthmüller.<sup>19</sup> We found the critical lattice parameters where a crossover from one magnetic state to another can occur.<sup>11</sup> In that study, a single unit cell consisting of eight atoms (four Mn and four P) was used, which allowed three different collinear antiferromagnetic configurations (AFM1,

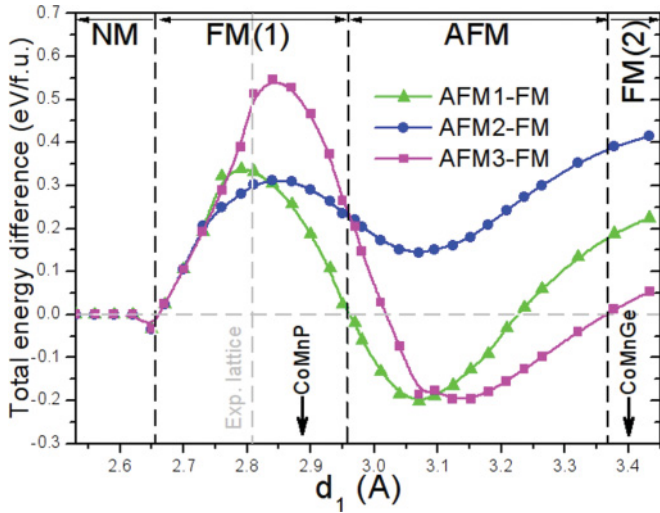


FIG. 1. (Color online) Stability of possible collinear magnetic structures, relative to ferromagnetism, within a single unit cell of MnP as a function of  $d_1$  Mn-Mn separation. AFM configurations become stable where  $\Delta E_{\text{AFM-FM}} < 0$ . The vertical dashed line represents the experimental (strain free,  $\varepsilon = 0$ ) lattice of MnP. We see that the FM state is first destabilised by lattice expansion, and then becomes stable again at large  $d_1$  values: FM(2).

AFM2, and AFM3) and a collinear ferromagnetic (FM) one to be constructed. In the interval of  $2.5 \text{ \AA} \lesssim d_1 \lesssim 3.22 \text{ \AA}$  we were able to predict a transition in the zero temperature magnetic structure from NM to FM, and finally to AFM as a function of expanding lattice parameters. A detailed description of the DFT calculations is given in that work<sup>11</sup>. Here we extend our simple binary model to  $d_1 > 3.22 \text{ \AA}$  values by further hydrostatic expansion in order to interpret ferromagnetism in CoMnGe where  $d_1 = 3.4 \text{ \AA}$  in the current model.

Figure 1 shows the difference in energy between the possible collinear AFM and FM magnetic states ( $\Delta E_{\text{Tot}} = E_{\text{AFM}} - E_{\text{FM}}$ ) as a function of Mn-Mn separation. Using this comparison scheme a non-FM state becomes most favorable when it has the most negative value of  $\Delta E_{\text{Tot}}$ . On the left-hand side of Fig. 1, the large compression causes a strong overlap of  $d$  orbitals, and the broad  $d$ - $d$  hybrid bands thus formed cannot support spontaneous magnetization. In agreement with experimental findings, the FM state is the ground state of MnP and is stable for intermediate deformations of the lattice. On further expansion of the lattice parameters, first the AFM1-type magnetic structure (at around  $d_1 \sim 2.97 \text{ \AA}$ ) and then the AFM3-type ordering (at  $d_1 \sim 3.1 \text{ \AA}$ ) become energetically favorable. However the extended study presented here shows that AFM3-type ordering ceases to be the most stable magnetic state for large lattice expansion, and eventually the collinear FM state is once again the ground state for  $d_1 \gtrsim 3.37 \text{ \AA}$ .

In order to experimentally prove the validity of the model, we carefully selected two collinear FM compositions with lattice parameters from the different FM regions of the stability plot in Fig. 1. Our choices were CoMnP from the FM(1) regime ( $d_1 \sim 2.95 \text{ \AA}$ <sup>20</sup>) and CoMnGe ( $d_1 \sim 3.4 \text{ \AA}$ <sup>3</sup>) from the larger Mn-Mn separation (FM2) zone. Our hypothesis is that progressive substitution of one  $p$  element for another in  $\text{CoMnGe}_{1-x}\text{P}_x$ , without changing the  $3d$ -element

TABLE I. Calculated magnetic moments ( $\mu_B$ ) and  $N_{\text{Tot}}(E_{\text{F}})$  (states/eV/f.u.) for  $\text{CoMnGe}_{1-x}\text{P}_x$ .

$x$	$M_{\text{Mn}}$	$M_{\text{Co}}$	$M_{\text{Si/Ge}}$	$M_{\text{Tot}}$	$N_{\text{Tot}}(E_{\text{F}})$
0	3.05	0.6	-0.07	3.58	5.0
0.25	2.83	0.45	-0.06	3.22	10.0
0.5	2.89	0.47	-0.07	3.29	9.5
0.75	2.71	0.33	-0.07	2.97	7.5
1	2.68	0.28	-0.07	2.89	1.7

concentration, can cause the appearance of metamagnetism in particular compositions of the series. This replacement of large germanium atoms by the much smaller phosphor atoms should result in a shrinkage of lattice. From Fig. 1 we expect that the decreasing  $d_1$  separation will lead to the destabilization of FM state in competition with the AFM one at a certain P/Ge ratio. It should then be possible to manipulate the magnetic state of the energetically metastable alloys by changing temperature or applied magnetic field.

In order to identify the key factors that can lead to the substantial changes in magnetic ground state, we first calculate the electronic band structure and magnetic moment of  $\text{CoMnGe}_{1-x}\text{P}_x$  alloys with  $x = 0, 0.25, 0.5, 0.75$ , and 1 in a collinear FM state. The calculated magnetic moments are given in Table I. The magnetic moments on Mn ( $2.68 \mu_B$ ) and Co ( $0.28 \mu_B$ ) sites in the CoMnP alloy agrees well with previous calculations based on the KKR method with coherent potential approximation (CPA) by Zach and co-workers.<sup>21</sup> Furthermore, the partial replacement of P by Ge results in a progressive increase of magnetic moment on both  $3d$  elements, leading to an increased  $M_{\text{Tot}}$  of up to  $3.58 \mu_B$  for CoMnGe. A small negative moment induced on the  $p$ -block elements is also observed.

The FM total density of electronic states (DoS) of the two end compositions, CoMnP and CoMnGe, are plotted, together with  $\text{CoMnP}_{0.5}\text{Ge}_{0.5}$  in Fig. 2. Although the value of total density of states at the Fermi level,  $N_{\text{Tot}}(E_{\text{F}}) = N_{\downarrow}(E_{\text{F}}) + N_{\uparrow}(E_{\text{F}})$  exhibits a large change with composition, each total DoS possesses the same features over a large extent of energy range. The main difference is the location of these features, and in particular the location of a pseudogap-like feature in the DoS. Using CoMnP as reference, if the energy scale of the minority DoS is shifted by about  $+0.25 \text{ eV}$  for CoMnGe and about  $-0.3 \text{ eV}$  for  $\text{CoMnP}_{0.5}\text{Ge}_{0.5}$ , not only would the pseudogap fall at  $E_{\text{F}}$  but most of the exchange-split DoS peaks of Mn and Co would line up at around the same position. The large  $N_{\text{Tot}}(E_{\text{F}})$  in  $\text{CoMnP}_{0.5}\text{Ge}_{0.5}$  (Table I) suggests the instability of the collinear FM state in this composition. A possible scenario that stabilizes the noncollinear state through the formation of hybridization gap at the Fermi energy is described by Lizárraga *et al.*<sup>8</sup> We recently showed the relevance of this mechanism in a noncollinear DFT study on the metamagnet  $\text{CoMnSi}$ .<sup>10</sup>

In the following sections, we are going to demonstrate the validity of our theoretical prediction of metamagnetism in these Mn-based  $Pnma$  alloys through magnetic and structural results on an experimentally synthesized  $\text{CoMnGe}_{1-x}\text{P}_x$  series of alloys.

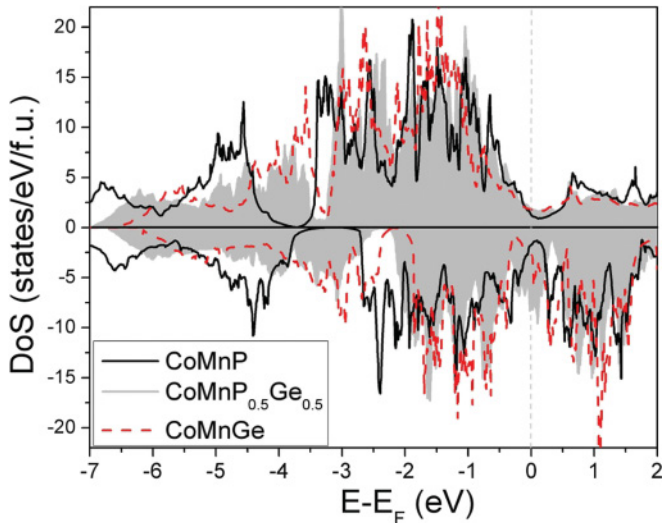


FIG. 2. (Color online) Collinear FM total density of states for  $\text{CoMnGe}_{1-x}\text{P}_x$  with  $x = 0, 0.5$ , and  $1$ . The Fermi energy falls into the hybridization gap for both  $\text{CoMnP}$  and  $\text{CoMnGe}$ , but shifted for  $\text{CoMnP}_{0.5}\text{Ge}_{0.5}$  resulting in a large  $N_{\text{Tot}}(E_{\text{F}})$ .

### III. EXPERIMENTAL

#### A. Experimental details

Samples of  $\text{CoMnGe}_{1-x}\text{P}_x$  with  $x = 0.25, 0.4, 0.5, 0.55, 0.6$ , and  $0.75$  were prepared in a quartz nozzle by an induction melting technique, using  $\text{Co}_2\text{P}$  (99.9%) and  $\text{Mn}_3\text{P}_2$  (99.9%) master alloys mixed together with high-purity  $\text{Co}$  (99.97%),  $\text{Mn}$  (99.99%), and  $\text{Ge}$  (99.9999%) elements in the required proportions. The alloys were cast into a copper mold under protective Ar atmosphere. The ingots were then sealed in quartz tube under protective He atmosphere and a homogenization at  $1000^\circ\text{C}$  for 24 h and annealing treatment at  $800^\circ\text{C}$  for 72 h then followed. The samples thus obtained were crushed into fine powder in order to determine their crystal structure using x-ray diffraction (XRD) with  $\text{Cu } K\alpha$  radiation. Structural (Rietveld) refinement of the data was carried out using the FULLPROF<sup>22</sup> program. A microstructural and compositional analysis was carried out using a Carl Zeiss 1540EsB scanning electron microscope (SEM). Magnetic properties of the samples were studied in a Quantum Design MPMS system.

#### B. Crystal structure

Both  $\text{CoMnGe}$  and  $\text{CoMnP}$  alloys crystallize in the orthorhombic ( $Pnma$ , 62) structure in which the elements occupy general  $4c$  ( $x, \frac{1}{4}, z$ ) crystallographic positions. XRD analysis of the  $\text{CoMn}(\text{Ge},\text{P})$  samples revealed the formation of this orthorhombic structure in all compositions. Furthermore, in the samples with  $x = 0.25, 0.4, 0.5$ , and  $0.75$ , extra reflections in the diffraction pattern also appear that can be ascribed to the hexagonal  $\text{Ni}_2\text{In}$ -type ( $P6_3/mmc$ , 194) lattice structure. The appearance of the higher symmetry hexagonal phase is often observed in similar alloy systems because the orthorhombic structure can be regarded as a distortion from this hexagonal structure and the two structures can be interrelated as follows:  $b_{\text{ortho}} = a_{\text{hex}}$  and  $c_{\text{ortho}} = \sqrt{3} \times a_{\text{hex}}$ .

The importance of this latter correlation has been exploited in several Mn-based  $Pnma$  systems. In the pseudobinary  $\text{Mn}_{1-x}\text{Fe}_x\text{As}$  alloys the sharp, first order type magnetostructural transformation (orthorhombic  $\leftrightarrow$  hexagonal)<sup>23</sup> is also accompanied by a ‘‘colossal’’ MCE.<sup>24</sup> The magnitude of the useful magnetic entropy change is, however, now strongly contested.<sup>25</sup> A similar magnetostructural transition in  $\text{CoMnGe}$ -based ternary compositions was reported by Kanomata and co-workers who observed a large,  $\sim 5.3\%$ , volume change.<sup>26,27</sup> Theoretical calculations also revealed that the Co vacancy-induced phase transformation is due to a high moment to low moment magnetic transition accompanied by a large magnetovolume effect originating from the change of the coupling distance between the principal magnetic atoms.<sup>28</sup> As an extension of this study, both Hamer<sup>16</sup> and Trung<sup>17,18</sup> recently demonstrated that the transitions can be fine-tuned by pseudoternary additives (Sn, B, or Cr elements) around room temperature for an enhanced magnetocaloric effect. The appearance of the hexagonal structure at room temperature in our samples can therefore be understood as a first order transformation from the low temperature orthorhombic structure to a high temperature hexagonal one.

In order to clarify the composition of the hexagonal phase, a representative secondary electron (SE) SEM micrograph was taken from the  $\text{CoMnGe}_{0.75}\text{P}_{0.25}$  alloy and is shown in Fig. 3(a). The two different structural regions are identified in accordance with the XRD results. EDX elemental mapping revealed that the two phases have substantially different atomic compositions. Our investigations show that the orthorhombic phase is poor in Ge (and consequently enriched in P) whereas the second phase is enriched in Ge and is therefore close in composition to stoichiometric  $\text{CoMnGe}$ . An atomic composition profile taken along the direction of the arrow indicated in Fig. 3(b) shows quantitatively the compositional difference between the two structures. These findings are direct evidence

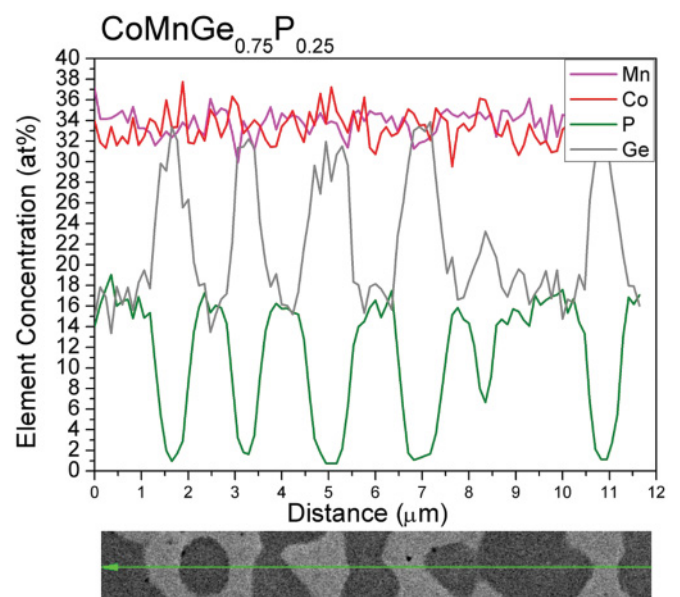


FIG. 3. (Color online) Representative SEM micrograph and corresponding elemental mapping from EDX of  $\text{CoMnGe}_{0.75}\text{P}_{0.25}$ .

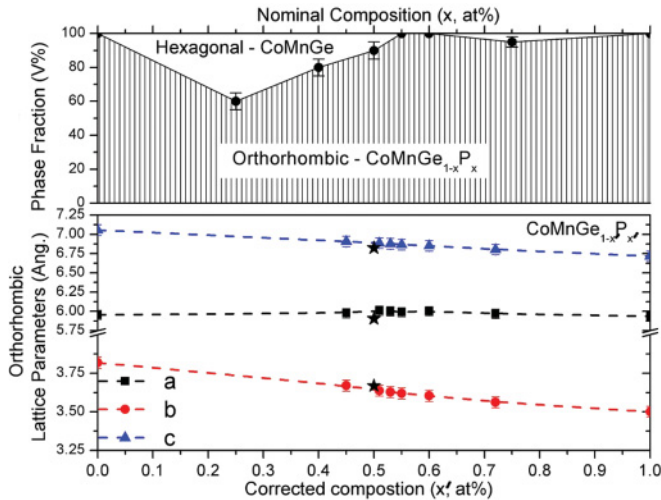


FIG. 4. (Color online) Volume fraction of the orthorhombic CoMnGe<sub>1-x</sub>P<sub>x</sub> and hexagonal CoMnGe phases as a function of nominal composition (top) and lattice parameters of the main orthorhombic phase as a function of corrected phosphor concentration (bottom). The lattice parameters of CoMnSi, a metamagnet, are added (star symbols) for comparison.

for a compositional phase separation of the quaternary alloy rather than for a second-order type transformation of the single quaternary composition with temperature.

The results of the quantitative Rietveld analysis in Fig. 4 (top) reveal the formation of single phase orthorhombic structures in the alloys rich in P ( $x > 0.5$ ). Figure 4 (bottom) summarizes the lattice parameter of the orthorhombic structure as a function P content. [The composition values ( $x'$ ) given in the lower figure are corrected based on the quantitative analysis.] The  $b$  and  $c$  lattice constants show decrease continuously with Ge addition while the  $a$  parameter stays nearly constant and until the lattice parameters with  $x \sim 0.5$  become close to those of the metamagnet CoMnSi.

In the next section, we will demonstrate the occurrence of metamagnetism in these Mn-based alloys that have appropriately designed lattice parameters.

### C. Magnetic properties

As we demonstrated in Sec. III B, the lattice parameters of the CoMnP<sub>1-x</sub>Ge<sub>x</sub> alloy can be tuned toward those of the CoMnSi metamagnet. In the present section, we will show that this structural engineering allows us to prepare metamagnetic quaternaries, even though the end alloys (CoMnP and CoMnGe) are ordinary ferromagnets. Based on the  $a$ ,  $b$ , and  $c$  lattice parameters of the CoMnGe<sub>1-x</sub>P<sub>x</sub> alloys, one would expect progressive change from collinear ferromagnetism to noncollinear antiferromagnetism with the replacement of P by Ge in the system. At around  $x \sim 0.5$  the structure should resemble that of the CoMnSi metamagnet and once the composition is on the P-rich end of the series, ferromagnetism should reappear. Indeed, we have found this scenario to be fulfilled; however the structural phase separation into a ternary CoMnGe and a residual CoMn(Ge,P) phase in compositions that are rich in Ge hinders a simple interpretation.

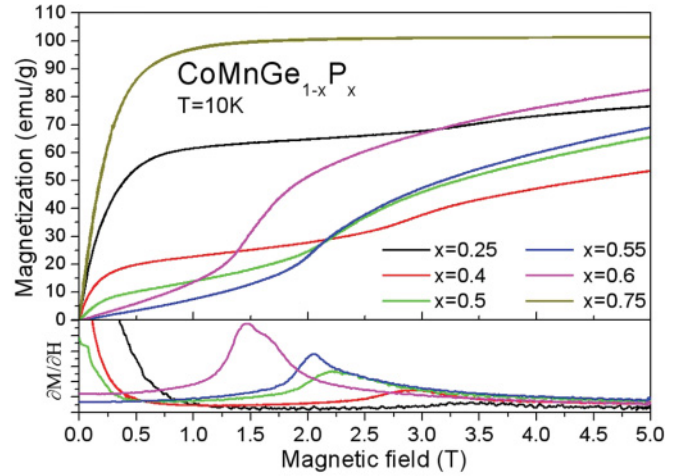


FIG. 5. (Color online) Magnetization loops of CoMnGe<sub>1-x</sub>P<sub>x</sub> at 10 K.

The composition dependence of magnetization loops taken at 10 K is shown in Fig. 5. Metamagnetism is most visible in the single phase compositions with  $x = 0.55$  and  $0.6$ . In these samples, the initial magnetization varies almost linearly with applied field below the inflection point that occurs at a critical field value. Although this critical behavior is also visible in all compositions with  $x \leq 0.6$ , the increasing volume of ferromagnetic CoMnGe phase at low  $x$  suppresses the sharpness of the upturn in magnetisation. A distinct shift of the peak of  $\frac{\partial M}{\partial H}$ , seen in Fig. 5(b) shows that the critical field decreases sharply as more Ge is replaced by P (towards small  $x$ ).

The composition dependence of the critical field in a field of 1 Tesla is shown in Fig. 6 and is consistent with the magnetisation loops collected at 10 K. The lower the critical field that is observed at 10 K (Fig. 5), the lower the critical temperature is at which the 1 T applied magnetic field is sufficiently large to bring the sample to the high-magnetic state. A strong dependence of the metamagnetic transition

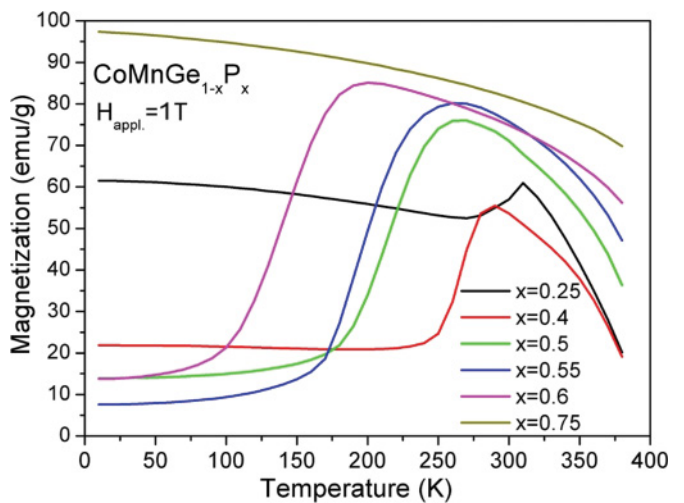


FIG. 6. (Color online) Isofield magnetization of CoMnGe<sub>1-x</sub>P<sub>x</sub> as a function of temperature, measured in a 1 Tesla applied field. We observe metamagnetism in almost all samples, and a sharp change in the metamagnetic critical temperature with composition in the range  $x = 0.4$  to  $0.6$ .

temperature on crystal structure is evident from this figure, when compared with Fig. 4. Although samples with  $x \leq 0.5$  contain a minor second phase, they all show a characteristic increase in the magnetization as a function of temperature, indicative of native metamagnetism. In the high Ge (low  $x$ ) side of the series, with  $x = 0.25$ , although the substantial ferromagnetic volume (from the  $\text{CoMnGe}$  phase) largely suppresses the metamagnetic transition, it still appears at around room temperature (RT).

As the samples become richer in phosphor, the critical temperature decreases sharply from  $\sim 300$  K to  $\sim 80$  K and it eventually disappears for  $x = 0.75$ . The highest magnetization values in a 1 T applied field show an increase with  $x$  (except for  $x = 0.25$ ) as the result of a balance of several effects. Firstly, it is easily foreseeable that at lower transition temperatures ferromagnetic configurations will exhibit larger overall net moments compared to those of the higher temperature ones. Secondly, the presence of the hexagonal  $\text{CoMnGe}$  lifts the low temperature “baseline” of magnetization in Fig. 6.

#### IV. SUMMARY AND CONCLUSIONS

Using DFT calculations based on a “prototype” binary MnP composition, we have investigated the occurrence of AFM and FM states in Mn-based orthorhombic ( $Pnma$ , 62) alloys. As the result of isotropic expansion, the FM(1) ground state is no longer stable but instead AFM coupling of the spins on the Mn atoms is predicted above  $d_1 \gtrsim 2.95$  Å.<sup>11</sup> In this work, we have extended our theoretical investigation to higher hydrostatic expansions and found the reoccurrence of ferromagnetism (FM2) at large Mn-Mn separations over  $d_1 \gtrsim 3.37$  Å that also explains the collinear ferromagnetism in  $\text{CoMnGe}$  with  $d_1 = 3.4$  Å.

Based solely on the deduced magnetic stability plot (Fig. 1), we designed a series of pseudoternary  $\text{CoMn}$ -based alloys in order to experimentally prove the validity of our theoretical concept. Taking two collinear FM ternaries: one,  $\text{CoMnP}$  with a low  $d_1$  from the FM1 region; the other,  $\text{CoMnGe}$  with a

high  $d_1$  from the FM2 region we attempted to drive the alloy magnetism toward the metamagnetic/AFM zone by careful structural design.

The experimental investigation of  $\text{CoMnGe}_{1-x}\text{P}_x$  has indeed revealed an AFM ground state for compositions  $x \approx 0.5$ . The appearance of a magnetic field- and temperature-dependent metamagnetic transition in several samples also suggests the existence of complex noncollinear spin structure in most of them, and in particular in the range  $x = 0.4$  to  $0.6$ . The large predicted  $N_{\text{Tot}}(E_{\text{F}})$  for  $x = 0.5$  (in Sec. II) in a hypothetical FM state is because of a shift in the energy of the hybridisation-derived pseudogap as the lattice parameters expand upon Ge substitution for phosphor.

Although the complex magnetic spin structure of these new samples is to be determined, the system is an example of the stabilization of noncollinear magnetism through the formation of hybridization gap at the Fermi energy as described by Lizárraga *et al.*<sup>8</sup> and as recently found in the ternary  $\text{CoMnSi}$ .<sup>10</sup> The Mn-containing  $Pnma$  structure is extremely versatile with regard to elemental substitution. The above demonstration of a structurally directed tuning of magnetic properties therefore provides a potential direction for future tailoring of metamagnetic phase transitions toward their use in applications such as those that rely on the magnetocaloric effect.

#### ACKNOWLEDGMENTS

Z.G. is grateful for the invitation and financial support of NIMS through the Open Research Institute Program. K.G.S. acknowledges financial support from The Royal Society. Furthermore, the authors thank H. S. Amin for his assistance in the SEM sample preparation and analysis. The research leading to these results has received funding from the European Community’s 7th Framework Programme under grant agreement no. 214864 (“SSEEC”). Computing resources provided by Darwin HPC and Camgrid facilities at The University of Cambridge and the HPC Service at Imperial College London are gratefully acknowledged.

<sup>1</sup>T. Nagamiya, *Solid State Phys.* **20**, 305 (1967).

<sup>2</sup>A. Kallel, H. Boller, and E. Bertaut, *J. Phys. Chem. Solids* **35**, 1139 (1974).

<sup>3</sup>S. Nizioł, A. Bombik, W. Bazela, A. Szytuła, and D. Fruchart, *J. Magn. Magn. Mater.* **27**, 281 (1982).

<sup>4</sup>T. Eriksson, L. Bergqvist, T. Burkert, S. Felton, R. Tellgren, P. Nordblad, O. Eriksson, and Y. Andersson, *Phys. Rev. B* **71**, 174420 (2005).

<sup>5</sup>S. Nizioł, H. Binczycka, A. Szytuła, J. Todorovic, R. Fuchart, J. Senateur, and D. Fruchart, *Phys. Status Solidi A* **45**, 591 (1978).

<sup>6</sup>L. Dobrzynski and A. Andresen, *J. Magn. Magn. Mater.* **82**, 67 (1989).

<sup>7</sup>R. J. Elliott and F. A. Wedgwood, *Proc. Phys. Soc.* **81**, 846 (1963).

<sup>8</sup>R. Lizárraga, L. Nordström, L. Bergqvist, A. Bergman, E. Sjöstedt, P. Mohn, and O. Eriksson, *Phys. Rev. Lett.* **93**, 107205 (2004).

<sup>9</sup>K. G. Sandeman, R. Daou, S. Özcan, J. Durrell, N. Mathur, and D. Fray, *Phys. Rev. B* **74**, 224436 (2006).

<sup>10</sup>A. Barcza, Z. Gercsi, K. S. Knight, and K. G. Sandeman, *Phys. Rev. Lett.* **104**, 247202 (2010).

<sup>11</sup>Z. Gercsi and K. G. Sandeman, *Phys. Rev. B* **81**, 224426 (2010).

<sup>12</sup>H. Fjellvåg, A. Andresen, and K. Bärner, *J. Magn. Magn. Mater.* **46**, 29 (1984).

<sup>13</sup>B. Sredniawa, R. Zach, P. Fornal, R. Duraj, A. Bombik, J. Tobola, S. Kaprzyk, S. Nizioł, D. Fruchart, M. Bacmann *et al.*, *J. Alloys Compd.* **317–318**, 266 (2001).

<sup>14</sup>W. Bazela, A. Szytuła, J. Todorovic, and A. Zieba, *Phys. Status Solidi* **64**, 367 (1981).

<sup>15</sup>V. Johnson, *Inorg. Chem.* **14**, 1117 (1975).

<sup>16</sup>J. Hamer, R. Daou, S. Özcan, N. Mathur, D. Fray, and K. G. Sandeman, *J. Magn. Magn. Mater.* **321**, 3535 (2009).

<sup>17</sup>N. T. Trung, V. Biharie, L. Zhang, L. Caron, K. H. J. Buschow, and E. Bruck, *Appl. Phys. Lett.* **96**, 162507 (2010).

<sup>18</sup>N. T. Trung, L. Zhang, L. Caron, K. H. J. Buschow, and E. Bruck, *Appl. Phys. Lett.* **96**, 172504 (2010).

- <sup>19</sup>G. Kresse and J. Furthmüller, *Phys. Rev. B* **54**, 11169 (1996).
- <sup>20</sup>D. Fruchart, M. Backmann, and P. Chaudouet, *Acta Crystallogr. Sect. B* **36**, 2759 (1980).
- <sup>21</sup>R. Zach, J. Tobola, B. Sredniawa, S. Kaprzyk, M. Guillot, D. Fruchart, and P. Wolfers, *J. Phys. Condens. Matter* **19**, 376201 (2007).
- <sup>22</sup>J. Rodríguez-Carvajal, *Phys. B Condens. Matter* **192**, 55 (1993).
- <sup>23</sup>H. Fjellvag, A. Kjekshus, A. F. Andresen, and A. Zieba, *J. Magn. Mater.* **73**, 318 (1988).
- <sup>24</sup>A. de Campos, D. Rocco, A. Magnus, G. Carvalho, L. Caron, A. Coelho, S. Gama, L. da Silva, F. Gandra, A. dos Santos *et al.*, *Nat. Mater.* **5**, 802 (2006).
- <sup>25</sup>M. Balli, D. Fruchart, D. Gignoux, and R. Zach, *Appl. Phys. Lett.* **95**, 072509 (2009).
- <sup>26</sup>T. Kanomata, H. Ishigaki, T. Suzuki, H. Yoshida, S. Abe, and T. Kaneko, *J. Magn. Mater.* **140–144**, 131 (1995).
- <sup>27</sup>K. Koyama, M. Sakai, T. Kanomata, and K. Watanabe, *Jpn. J. Appl. Phys.* **43**, 8036 (2004).
- <sup>28</sup>J.-T. Wang, D.-S. Wang, C. Chen, O. Nashima, T. Kanomata, H. Mizuseki, and Y. Kawazoe, *Appl. Phys. Lett.* **89**, 262504 (2006).